

pubs.acs.org/JACS Article

Cyclic and Linear Tetrablock Copolymers Synthesized at Speed and Scale by Lewis Pair Polymerization of a One-Pot (Meth)acrylic Mixture and Characterized at Multiple Levels

Ryan W. Clarke, Maria Rosaria Caputo, Lucas Polo Fonseca, Michael L. McGraw, Liam T. Reilly, Kevin A. Franklin, Alejandro J. Müller,* and Eugene Y.-X. Chen*



ABSTRACT: Cyclic block copolymers (${}^{\circ}BCP$) are fundamentally intriguing materials, but their synthetic challenges that demand precision in controlling both the monomer sequence and polymer topology limit access to AB and ABC block architectures. Here, we show that cyclic ABAB tetra-BCPs (${}^{\circ}ABAB$) and their linear counterpart (${}^{l}ABAB$) can be readily obtained at a speed and scale from one-pot (meth)acrylic monomer mixtures, through coupling the Lewis pair polymerization's unique compounded-sequence control with its precision in topology control. This approach achieves fast (${}^{\circ}ABAB$) and quantitative (${}^{\circ}ABAB$) conversion to tetra-BCPs of predesignated linear or cyclic topology at scale (${}^{\circ}ABAB$) in a one-pot procedure, precluding the needs for repeated chain extensions, stoichiometric addition steps, dilute conditions, and postsynthetic modifications, and/or postsynthetic ring-closure steps. The resulting ${}^{l}ABAB$ and ${}^{\circ}ABAB$ have essentially identical molecular weights (${}^{\circ}BABB$) and block degrees/symmetry, allowing for direct behavioral comparisons in solution (hydrodynamic volume, intrinsic viscosity, elution time, and refractive indices), bulk (thermal transitions), and film (thermomechanical and rheometric properties and X-ray scattering patterns) states. To further the morphological characterizations, allylic side-chain functionality is exploited via the thiol—ene click chemistry to install crystalline octadecane side chains and promote phase separation between the A and B blocks, allowing visualization of microdomain formation.

■ INTRODUCTION

Cyclic polymers are intriguing materials, in comparison to their linear counterparts. Owing to their lack of chain-end functionality, loss of conformational freedom, and reduced chain-entanglement factors, cyclic polymers exhibit distinct macromolecular behavior in solution, film, and bulk settings. In solution, cyclic polymers have lower viscosity ([η]), smaller hydrodynamic volume ($V_{\rm h}$), radius of gyration ($R_{\rm g}$), lower refractive index (dn/dc), and lower density (ρ). Impacts on thermal properties include higher glass transition ($T_{\rm g}$) and decomposition ($T_{\rm d}$) temperatures as well as enhanced rate of crystallization, temperatures as well as enhanced rate of crystallization, which coupled with lower melt viscosity than linear analogues by bulk rheology measurements, provide complementary attributes for accessible processing of rigid polymers. Thus, control over

polymer topology presents itself as a synthetic handle for finetuning material performance, exploring new material potentials, and promoting cyclic polymer application.

Currently, cyclic block copolymers (°BCPs) are limited to AB and ABC architectures due to demanding requirements in synthetic approaches, of which few strategies have been reported.^{23–30} When obtained, however, 'BCPs offer new self-

Received: December 14, 2023 Revised: January 21, 2024 Accepted: January 25, 2024 Published: February 12, 2024





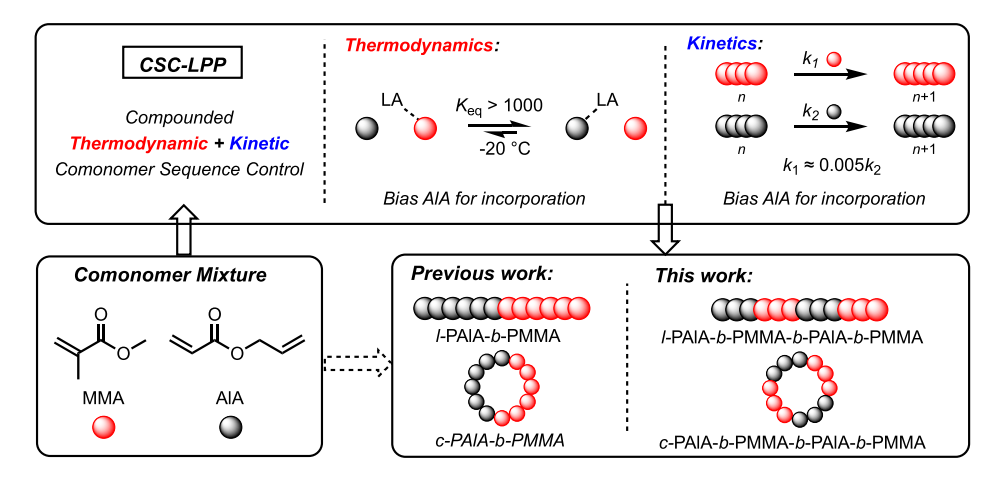


Figure 1. Compounded thermodynamic and kinetic comonomer sequence control in CSC-LPP for producing symmetrical and DP-precise linear and cyclic tetra-BCPs.

assembly behavior and microdomain formation distinguished from well-studied linear block copolymer (BCP) counterparts by transmission electron microscopy (TEM) and small-angle X-ray scattering (SAXS). Specifically, well-defined linear and cyclic ABC tri-BCPs of polyisoprene-b-polystyrene-bpoly(2-vinylpyridine) carefully prepared under low-temperature anionic polymerization, high vacuum, and multistep postfunctionalization for bimolecular ring closure have been subjected to thorough investigation by Hadjichristidis et revealing a shift from hexagonally close-packed coreshell cylinders in the linear topology to a rather unique wormlike morphology for the cyclic counterpart. As an example of 'BCPs for lithographic applications, 'ABC tri-BCP polybutadiene-b-polystyrene-b-poly(methyl methacrylate) self-assembles into nanorings for ion etching on silica.³⁴ While additional synthetic routes such as ring-expansion, zwitterionic, anionic, and uni/bimolecular couplings are reported, obtaining 'BCPs in high purity and molecular weight from compatible comonomers remains a significant challenge. A simple and robust synthetic protocol may enable future adoption and application of the unique features expressed by 'BCPs.

Access to multiblock copolymers (MBCPs) beyond traditional AB, ABA, and ABC block architectures has garnered high interest for advancing functional materials in nanotechnology^{35,36} and biomedical applications.³⁷ Increasing the number of blocks along a polymer chain results in a higher degree of interdomain crossings and chain entanglement "anchor" points, thus increasing interfacial adhesion and improving mechanical performance. 38,39 For example, recently reported ABAB tetra-BCPs of polyethylene (PE) and itpolypropylene (iPP) revealed a dramatic increase in PE and iPP (otherwise immiscible) blend compatibility and mechanical performance over those treated with a ^lAB di-BCP. ^{40,41} Similarly, ABA tri-BCPs phase separate into networks wherein A-domains are anchored to other A-domains through the middle B-block. This interdomain connectivity gives the material thermoplastic elastomer (TPE) behavior otherwise absent in the analogous AB-diblock. Initially, we set out to make cyclic-TPE polymers but realized that ABA architectures are not feasible for cyclic polymers, as they revert to AB after ring closing. Thus, it seems the minimum complexity needed to obtain TPE behavior (i.e., interdomain network connectivity) from cyclic polymers is an ABAB-tetrablock. However, to the best of our knowledge, there are no reports

on ^cABAB BCPs (Figure 1) or their application due to challenging synthetic and separation requirements via conventional catalytic means. ⁴²

Recently, our group developed a compounded sequence control Lewis pair polymerization (CSC-LPP)⁴³ to copolymerize mixed-feed homologous polar vinyl monomers into well-defined cyclic di-BCPs in one-pot and one-step. 44 The unique two-step propagation mechanism of LPP, 45 wherein both steps (monomer activation and conjugate addition) are distinctly selective and compounding, enables comonomer sequence control over even isomeric monomer mixtures with high block resolution. Using CSC-LPP, we have learned that a unique alkyl sorbate-based ion pair can be used to yield precise and discrete 'BCPs absent of linear contaminants and premature ring-closure events without high dilution requirements.44 In a later work, we put forth several lines of mechanistic evidence for the cyclization mechanism in which we found Lewis acid (LA) involvement in the cyclization event itself.46 We hypothesized that free monomer discourages premature cyclization by saturating the LA thereby adding an additional degree of temporal control over cyclization. In this prior 'BCP work, 44 high preferential coordination (K_{eq}) of encumbered LA methylaluminum bis(2,6-di-tert-butyl-4-methylphenoxide) (MAD) to *n*-butyl acrylate (ⁿBA) over methyl methacrylate (MMA) was exploited to restrict MMA from the propagation cycle until "BA depletion. This effect compounded with a heavily biased rate of propagation (k_p) toward "BA allowed for rapid consumption of "favorable" "BA prior to "unfavorable" MMA with an infinitesimal margin for misincorporation. In this work, we reasoned that we could add a second feed of the favorable monomer (A, in this case ⁿBA) during some predesignated concentration of the unfavorable monomer (B, in this case MMA), thus immediately shifting coordination (K_{eq}) and propagation (k_p) back to A to obtain a 'ABAB tetra-BCP upon full conversion of both A and B. The time-point for addition can be selected with high precision by first preparing and tracking parent di-BCP polymerization kinetics. Such a system would achieve 'ABAB in a speedy and convenient one-pot, two-step fashion.

We thus herein present the results of our rapid and scalable tetra-BCP synthetic strategy while highlighting several behavioral differences between linear and cyclic topological analogues of di- and tetra-BCPs. We individually characterize these materials with nearly identical number-average molecular weight $(M_n \sim 165 \text{ kg mol}^{-1})$, degree of polymerization (DP) of blocks (DP of A and B = \sim 500 total each), and symmetry (architecturally), in two ways: (1) linear vs cyclic topology analogues and (2) di- vs tetra-BCP compositional analogues. The behavioral contrasting between these constitutionally isomeric BCPs is probed by solution ($[\eta]$, V_h , dn/dc, and elution time) measurements, bulk thermal (T_g and T_d), thermomechanical (dynamic modulus, tensile), and rheological (bulk viscosity) experiments (linear vs cyclic). Materials brought to the film stage were analyzed by X-ray scattering and/or electron microscopy experiments for topological confirmation, self-assembly assessment, and domain sizing as a key strategy to discriminate BCPs of similar composition yet varied architectures (di- vs tetra-BCPs).

RESULTS AND DISCUSSION

One-Pot Synthesis of Linear and Cyclic Tetra-BCPs **Enabled by CSC-LPP.** We designed two convergent polymerization methods to achieve compositionally identical cyclic and linear MBCP analogues requiring only a change in the initiating species to designate topology. Specifically, Lewis base (LB) tricyclohexylphosphine (PCy₃) was employed as the linear polymer initiator and ethyl sorbate/MAD/I^tBu (1,3-ditert-butylimidazol-2-ylidene) (1:1:1) ion pair 1 as the cyclic polymer initiator. 46 Monomers allyl acrylate (AlA) and MMA were selected for mixed-feed CSC-LPP due to their known high differentiation by $K_{\rm eq}$ (for the [M1]/[M2]/[LA] coordination equilibrium) and propagation rate $(k_{\rm p})$. 47 Using variable-temperature ¹H NMR to track the [AlA]/[MMA]/ [MAD] equilibrium at -20 °C, MMA/MAD coordination could not be observed, thus implying a heavy $K_{\rm eq}$ bias (>1000) for MAD preferential coordination to AlA over MMA (Figure S1). Additionally, the k_p for AlA was impressively high at $k_{p,obs}$ = $8.14 \times 10^4 \, [\mathrm{M}] \cdot \mathrm{s}^{-1} \cdot [\mathrm{LA}]_t^{-1} \cdot [\mathrm{LB}]_0^{-1}$, significantly higher than the recently reported $k_{p,obs} = 3.96 \times 10^2 [M] \cdot s^{-1} \cdot [LA]_t^{-1}$ [LB]₀⁻¹ for the LPP of MMA under nearly identical conditions (Figure S2).⁴⁷ The heavily biased equilibrium and kinetic values predict high sequence control for MAD-catalyzed LPP of this comonomer pair. Indeed, the one-pot CSC-LPP of this monomer pair showed rapid (<7 s) and complete consumption of AIA before MMA began to polymerize (Figure 2). From this kinetic profile, the time needed to achieve 50% conversion of MMA was measured to be about 156 s.

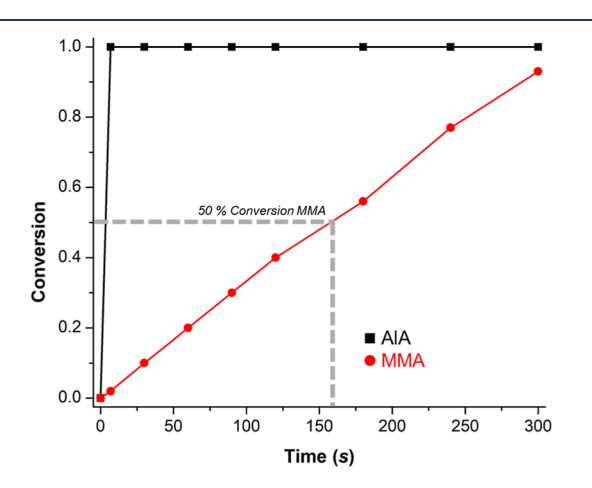


Figure 2. Kinetic conversion vs time plot tracking the one-pot CSC-LPP of AlA (black, DP = 500) and MMA (red, DP = 500).

To demonstrate our control of block symmetry while obtaining high-molecular-weight polymer, we targeted ABAB tetra-BCPs with DP = 250/250/250/250 for "A1/B1/A2/B2" blocks. To achieve this precision synthesis in the fewest possible addition steps, the addition of A2 monomer should occur at 50% conversion of B1, at which point the K_{eq} will immediately shift to promote polymerization of A2 over B2 (Figure 3). Two di-BCPs ('PAlA₅₀₀-b-PMMA₅₀₀ and ^lPAlA₅₀₀b-PMMA₅₀₀) were also synthesized at comparable monomer compositions prior to the tetra-BCPs, designed to both model kinetics and obtain baseline di-BCPs for comparison (Figure S3). As shown in Figure 2, the 50% conversion point of MMA during linear di-BCP synthesis occurred at 156 s, where AlA was quantitatively consumed before the first postinitiation time-point (<7 s).

Advancing to the ABAB sequence, the initial monomer feed was set to be AlA/MMA = 500:1000 expecting the first batch of AlA to quantitatively polymerize before the propagation of MMA could occur (Figures 2 and 3). Following injection of initiating species to each concurrently prepared linear and cyclic synthesis, a timer was started and monitored for precise addition of the second AlA feed. At the exact point of AlA (block A2) injection, an aliquot was taken from each polymerization to monitor the exact conversion of the MMA and assign block compositions. The 'ABAB AlA (A2) injection occurred at 51% MMA conversion, yielding 'PAlA250-b-PMMA₂₅₅-b-PAlA₂₅₀-b-PMMA₂₄₅ with a high block symmetry across the ring (Figures 3 and S4). The ¹ABAB synthesis achieved similar precision, with the addition of AlA at 55% MMA conversion to yield ¹PAlA₂₅₀-b-PMMA₂₇₅-b-PAlA₂₅₀-b-PMMA₂₂₅ (Figures 3 and S5). Sequencing and comonomer incorporation was evidenced by ¹H and ¹³C NMR, the latter revealing carbonyl regions visually well-resolved and characteristic of block architecture for both MMA and AlA signals (Figures S6-S13).

Differentiating between Linear and Cyclic Tetra-BCPs. First, we conducted gel permeation chromatography (GPC) to obtain the absolute molecular weights of each sample to ensure that we would be making appropriate comparisons across near-identical M_n species. Refractive indices (dn/dc) were measured in THF for each of the MBCPs. ABAB PAlA₂₅₀-b-PMMA₂₇₅-b-PAlA₂₅₀-b-PMMA₂₂₅ has a higher dn/dc of 0.0801 mL g⁻¹ than ABAB PAlA₂₅₀-b-PMMA₂₅₀ b-PMMA₂₇₅-b-PAIA₂₅₀-b-PMMA₂₅₀ with dn/dc = 0.0735 mL g^{-1} (Figures S14 and S15). This dn/dc trend was repeated for the di-BCPs, where the ¹PAlA₅₀₀-b-PMMA₅₀₀ registered 0.0783 mL g⁻¹, higher than and the cyclic analogue of 0.0764 mL g⁻¹ (Figures S16 and S17). These trends also support the differences in topology as cyclic polymers typically exhibit a lower refractive index than linear analogues. 11 With these values, we then obtained accurate absolute molecular weight values for the linear $(M_n = 165 \text{ kg mol}^{-1}, D = 1.25)$ and cyclic $(M_n = 168 \text{ kg mol}^{-1}, D = 1.18) \text{ tetra-BCPs (Figures 4A, S18,})$ and S19), as well as the linear $(M_n = 165 \text{ kg mol}^{-1}, D = 1.21)$ and cyclic ($M_n = 161 \text{ kg mol}^{-1}$, $\ddot{D} = 1.12$) di-BCPs (Figures S20 and S21).

As GPC separation sequences elution from high-to-low $V_{\rm h}$, cyclic polymers should elude later than linear analogues. When the MBCPs were examined in this context, our results agreed: the 'ABAB eluted at 20.4 min and the 'ABAB eluted at 20.8 min, despite the marginally higher molecular weight for 'ABAB (Figure 4A). Similarly, the 'AB eluded 0.6 min behind the linear analogue (Figures S18–S22A). As the cyclic architecture

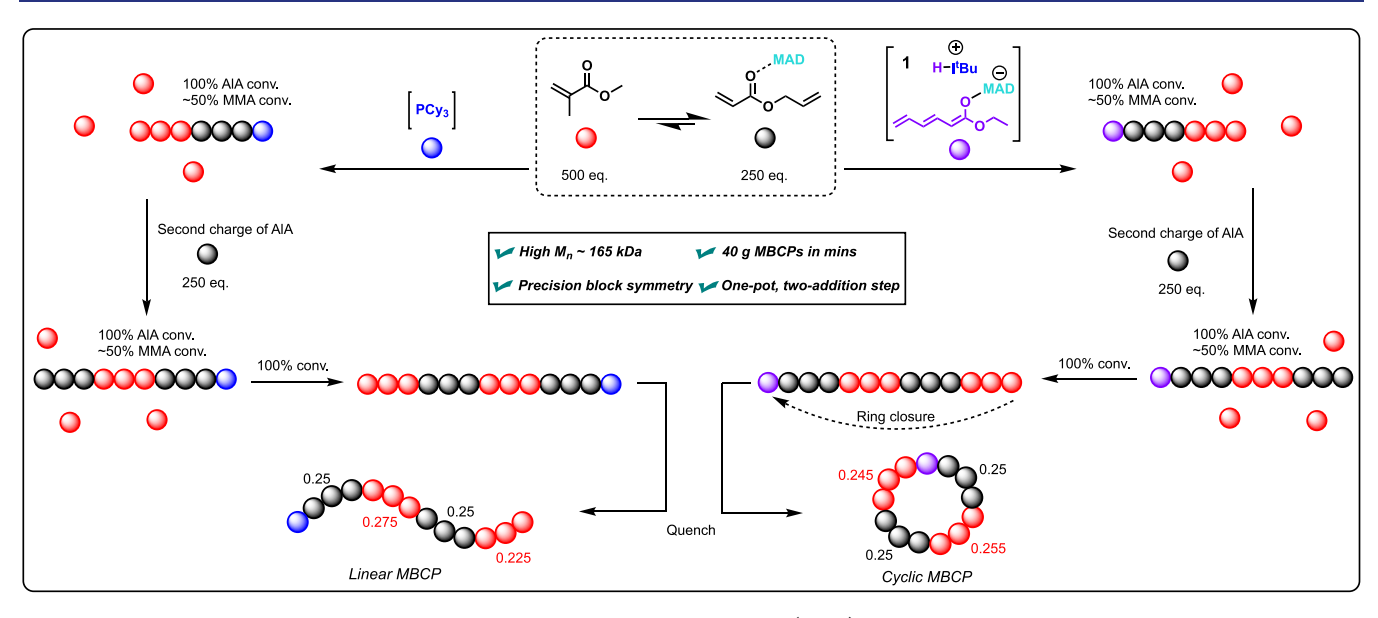


Figure 3. Outlined synthetic scheme for one-pot two-step CSC-LPP of homologous (meth)acrylic monomers to discrete and near-symmetric linear (left) and cyclic (right) ABAB tetra-BCPs (DP = 1000; 500 A total, 500 B total).

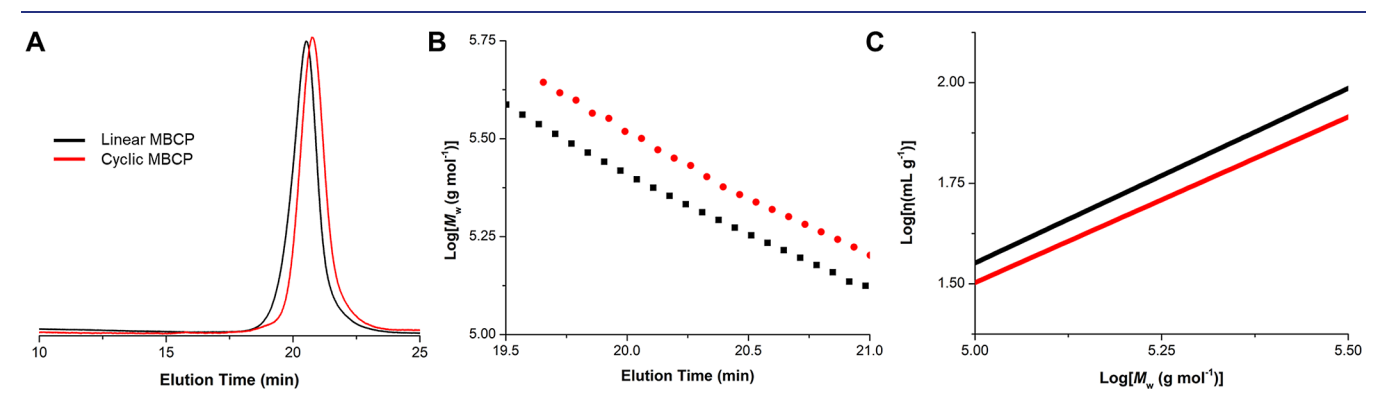


Figure 4. Overlays of chromatograms of: (A) GPC (dRI) traces, (B) $Log(M_w)$ vs normalized elution time plots, and (C) solution viscosity vs M_w plots for cyclic (red lines) and linear (black lines) tetra-BCPs, ${}^{\circ}PAlA_{250}$ -b-PMMA $_{255}$ -b-PAlA $_{250}$ -b-PMMA $_{245}$, and ${}^{l}PAlA_{250}$ -b-PMMA $_{275}$ -b-PAlA $_{250}$ -b-PMMA $_{225}$.

can pack more mass into less $V_{\rm h}$, it should also exhibit a higher molecular weight at the same elution time. When the molecular weights of the di- and tetra-BCPs are plotted logarithmically against standardized elution time, the cyclic architectures reveal a higher molecular weight per elution time than the linear architectures, further supporting topology assignments (Figures 4B and S22B).

Considering that linear polymers experience a higher degree of chain entanglement, solution viscosity should be higher than that of cyclic counterparts. In agreement, the viscosity of the ¹ABAB was higher than that of the cABAB (Figure 4C). This trend is consistent across the di-BCPs (Figure S22C). Overall, considering the demonstrated differences in elution time, refractive indices, elution molecular weights, and intrinsic viscosity, we collected converging evidence for differentiating topology and affirming topology for linear and cyclic tetra-BCPs with differing solution behavior.

Second, we focused on characterizing the differences in thermal behavior between the linear and cyclic ABAB tetra-BCPs. The chain-end groups in linear polymers are susceptible initiation sites for radical fragmentation events that ignite or expedite further thermal decomposition. These chain ends can be considered as defects in the repeat unit, which can decrease

the temperature for onset decomposition ($T_{\rm d,5\%}$). On the other hand, cyclic polymers have no chain-end sites and should thus exhibit higher $T_{\rm d,5\%}$ values and narrowed mass-loss profiles. In agreement, onset decomposition for the ^cABAB was recorded at 6 °C higher than that of the ^lABAB (Figures S23–S25). A higher onset was also observed for the ^cAB, occurring 8 °C higher than that of the ^lAB (Figures S26 and S27).

Like thermal degradation, cyclic polymers typically exhibit enhanced $T_{\rm g}$ values over their linear counterparts. In this case, differential scanning calorimetry (DSC) scans displayed a higher $T_{\rm g}$ for the 'ABAB in both the individual AlA and MMA blocks. For example, the PAlA-block $T_{\rm g}$ in the 'ABAB (–32 °C) is 3 °C higher than that in the ¹ABAB (–35 °C) (Figure S23). Similarly, the PMMA-block $T_{\rm g}$ in 'ABAB (121 °C) is 10 °C higher than that in ¹ABAB (111 °C) (Figures S28 and S29). These observations are consistent with thermal distinctions between the AB di-BCPs (Figures S30 and S31).

Third, on the basis of the reports that cyclic polymers exhibit a higher dynamic storage modulus (E') than that of linear analogues due to increased chain stiffness, we performed dynamic thermomechanical analysis (DTMA) via frequency sweeps (-50 to 200 °C, 5 °C/min, 1 Hz, 0.3%) for each material, recording E' as a function of temperature (Table S1).

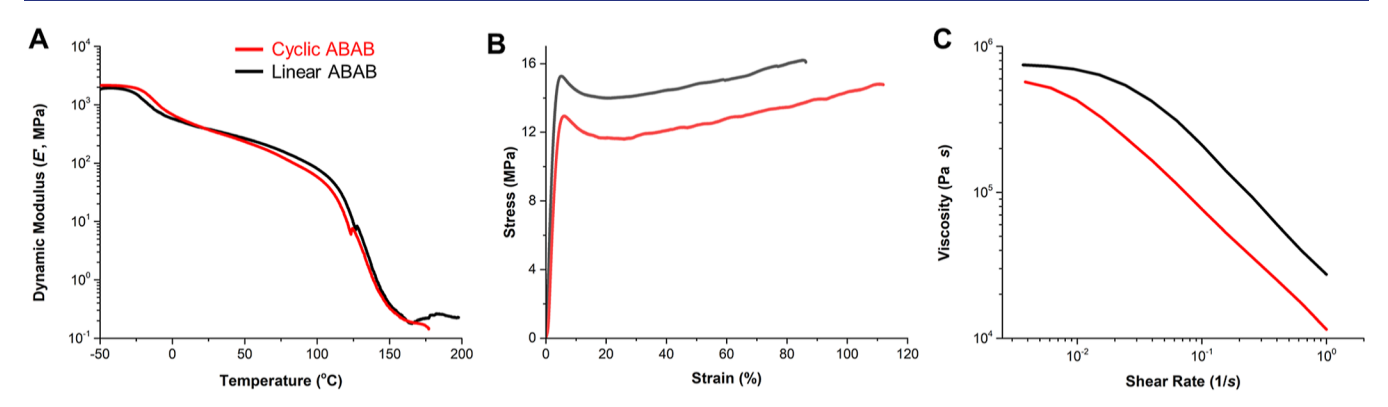


Figure 5. (A) DTMA temperature-ramp frequency curves (-50 to 200 °C, 5 °C/min, 0.3%, 1 Hz), (B) tensile stress/strain curves (room temperature, 5 mm/min), and (C) rheometric flow curves (175 °C, 10^{-3} to 1 s⁻¹, 10 rad/s) for linear (black, $M_n = 165$ kg mol⁻¹, D = 1.25) and cyclic (red, $M_n = 168$ kg mol⁻¹, D = 1.18) tetra-BCPs.

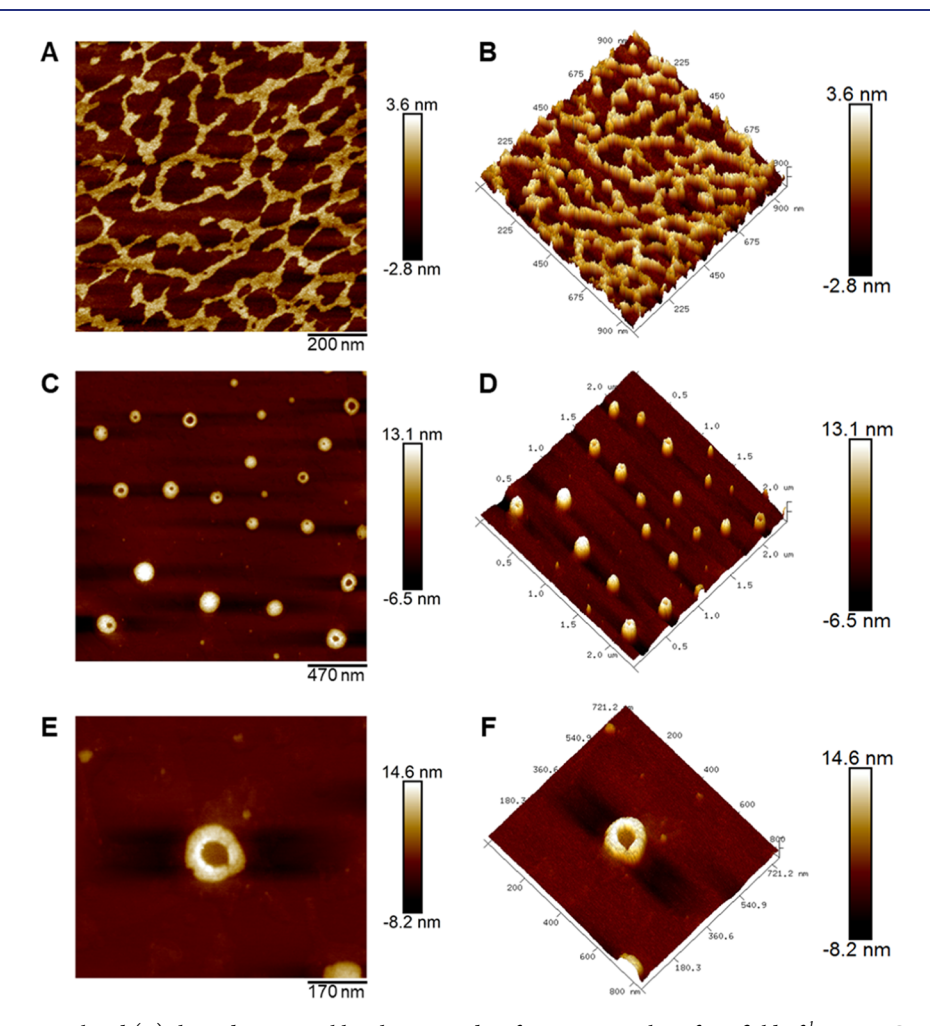


Figure 6. (A) Two-dimensional and (B) three-dimensional height sensor data from AFM analysis for a field of ¹ABAB BCPs. (C) Two-dimensional and (D) three-dimensional height sensor data from AFM analysis for a field of ¹ABAB BCPs. (E) Two-dimensional and (F) three-dimensional height sensor data from AFM analysis highlighting an individual ¹ABAB BCP aggregate.

The ¹ABAB showed $E'_{max} = 1.94$ GPa, notably lower than that of the ¹ABAB ($E'_{max} = 2.15$ GPa) (Figures 5A, S33, and S34). This topology-defined distinction is once more reflected in the ¹AB (2.44 GPa) and ¹AB (2.99 GPa) di-BCPs (Figures S35 and S36). We attribute these observations to the locked ring conformation in the cyclic polymers, which decreases the chain mobility. On the other hand, mechanical performances (Figure 5B) measured by uniaxial tensile testing revealed that the

'ABAB tetra-BCP showed somewhat lower ultimate tensile strength ($\sigma_{\rm B} \sim 15$ MPa) and Young's modulus ($E \sim 436$ MPa) but significantly higher ductility (elongation at break, $\varepsilon_{\rm B}$, ~112%), as compared to its linear counterpart ¹ABAB ($\sigma_{\rm B} \sim 16$ MPa, $E \sim 564$ MPa, $\varepsilon_{\rm B} \sim 73$ %).

Fourth, oscillatory shear rheology was next employed to distinguish flow-phase behavior. We specifically fixed on flow profiles, recording polymer viscosity as a function of shear rate

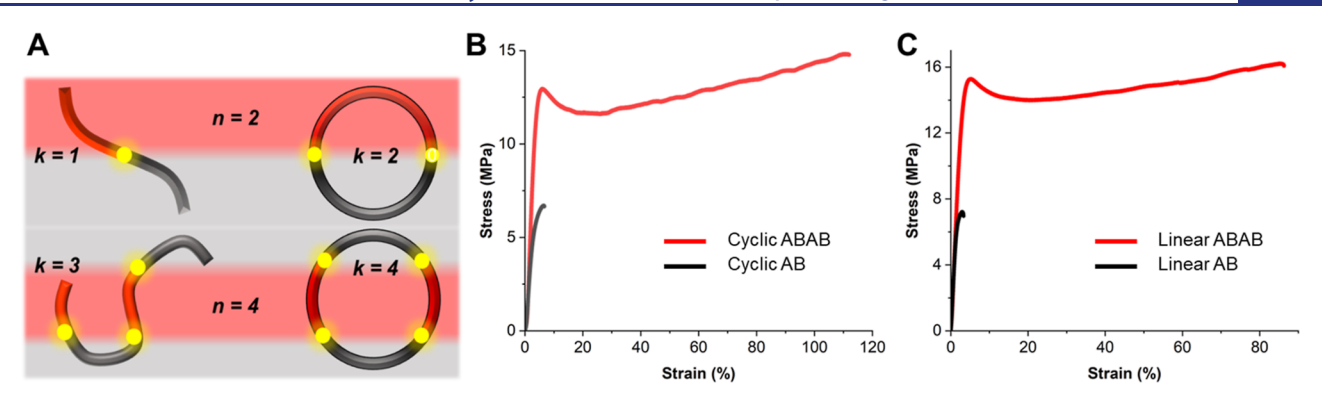


Figure 7. (A) Illustrative structural features of linear and cyclic AB di-BCPs and ABAB tetra-BCPs in the film phase considering self-assembly and interdomain chain penetrations (n = block count, k = cross-points). (B) Tensile stress/strain curves (room temperature, 5 mm/min) for cyclic AB di-BCP (black, $M_n = 161 \text{ kg mol}^{-1}$, D = 1.12) and ABAB tetra-BCP (red, $M_n = 168 \text{ kg mol}^{-1}$, D = 1.18). (C) Tensile stress/strain curves (room temperature, 5 mm/min) for linear AB di-BCP (black, $M_n = 165 \text{ kg mol}^{-1}$, D = 1.21) and ABAB tetra-BCP (red, $M_n = 165 \text{ kg mol}^{-1}$, D = 1.25).

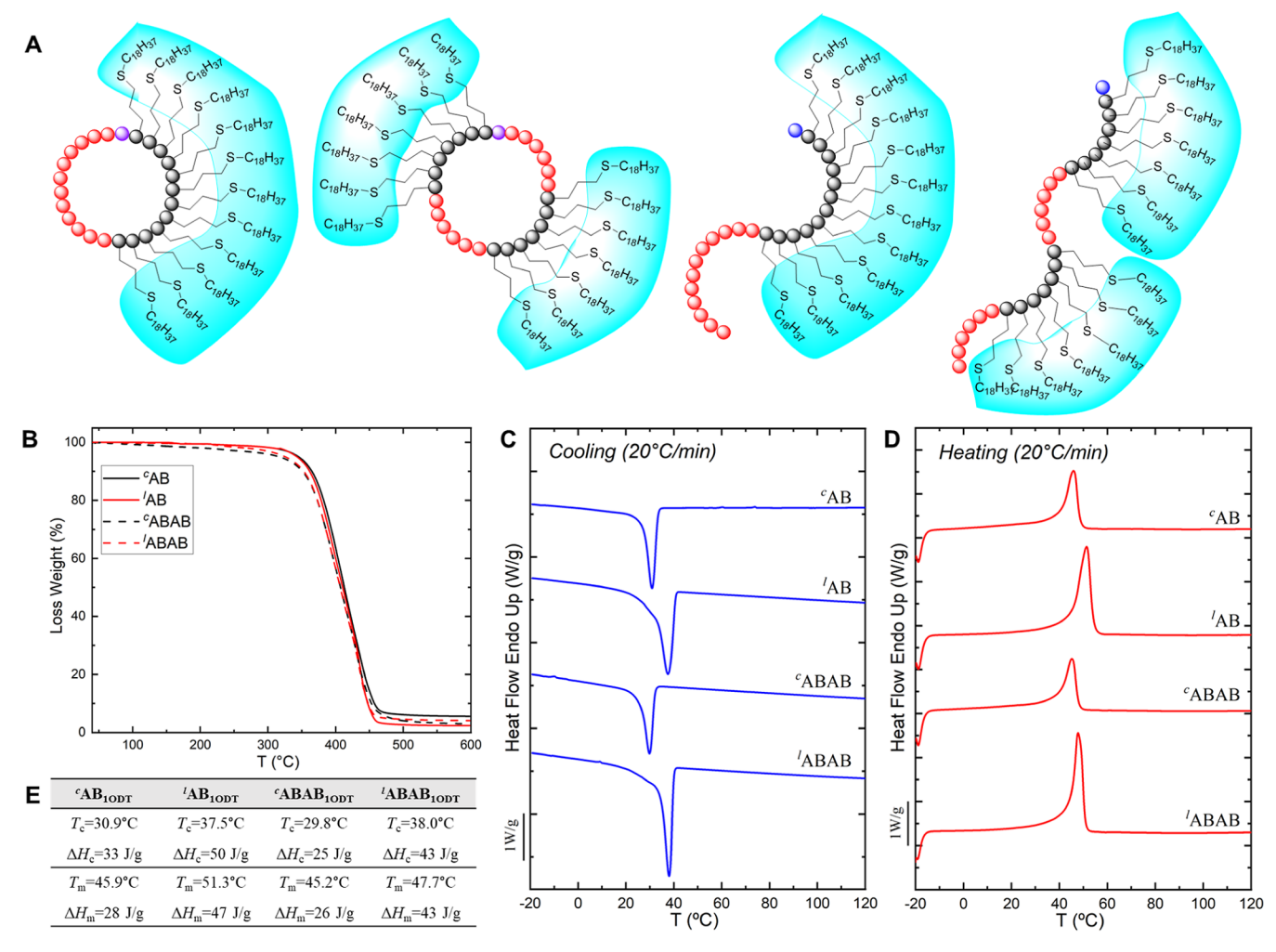


Figure 8. (A) Illustrative structures for the linear and cyclic di-BCP and tetra-BCP materials postfunctionalized via the thiol-ene click reaction with 1-ODT, with crystalline microdomain forming side-chains highlighted. (B) TGA plots for each BCP reveal a singular decomposition profile in the absence of the allylic side chain for PAIA. (C) DSC plots with observed T_c for each crystalline-grafted BCP species. (D) DSC plots with observed $T_{\rm m}$ for each crystalline-grafted BCP species. (E) Tabulated thermal events for each of the four semicrystalline BCPs (second heating scan at 20 °C/min, first cooling scan at 20 °C/min, -20 to 120 °C).

(175 °C, 10^{-3} to 1 s^{-1} , 10 rad/s) to observe the zero-shear viscosities and shear thinning behavior. Cyclic polymers should exhibit lower melt viscosities in view of their lower entanglement density, similar to solution behavior. In this case, both ^cBCPs (c AB = 232 × 10⁵ Pa s, ^cABAB = 572 × 10⁵

Pa s) exhibited lower melt viscosity than that of ^lBCPs (^lAB = $476 \times 10^5 \text{ Pa s}$, ¹ABAB = $749 \times 10^5 \text{ Pa s}$) (Figures 5C, S37– S40; Table S2). Architecturally, the ABAB tetra-BCPs exhibit zero-shear viscosity about 2× that of the AB di-BCPs, presumably due to increased interdomain chain entanglements.

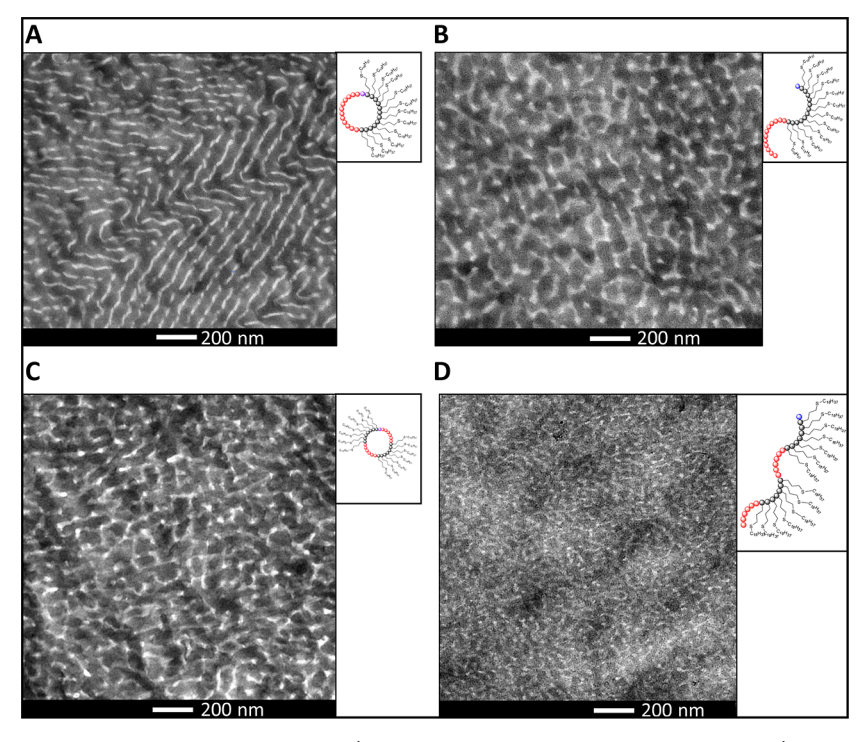


Figure 9. RuO₄-stained TEM images of: (A) 'AB di-BCP, (B) ¹AB di-BCP, (C) 'ABAB tetra-BCP, and (D) ¹ABAB tetra-BCP cryo-microtomed films.

The rate of shear-thinning was also evaluated, as we posit that the reduced chain entanglement factors for 'BCPs may affect the shear rate required to exhibit a thinning response. Accordingly, we measured the slope of the viscosity curve following the initial onset of shear thinning ($\sim 10^{-2} \text{ s}^{-1}$) (Figure 5C). Intriguingly, 'BCPs ('AB = -1.08x, 'ABAB = -0.82x) did not show rates of shear thinning that were faster than those of the 'BCP counterparts ('AB = -1.08x, 'ABAB = -0.80x) (Table S2). Instead, the rates of shear thinning behave more responsively to block count than topology, with increasing rates of shear thinning with increasing block complexity.

Fifth, most directly, atomic force microscopy (AFM) analysis conducted over solvent-casted (0.01 wt %) samples fully supported topological assignments of both tetra-BCP architectures (Figure 6). Micrographs of 'ABAB revealed ring morphologies with an average diameter of around 160 nm (Figures 6C-F and S41), while the corresponding ¹ABAB exhibited a completely different network-like morphology (Figures 6A,B and S42). Considering that the average degree of polymerization is 1000 for 'ABAB, and the average backbone length is around 0.22 nm per monomeric unit of MMA, 48 the diameters of the cycles obtained by AFM are within the size range of the 'ABAB. This agrees with the hypothesis that such cycles observed by AFM are composed of aggregates of cyclic macromolecules, which is also supported by the higher height (≈13 nm) verified for such cycles in the topography measurements, in comparison with the 'ABAB (\approx 4 nm) sample height. Therefore, interestingly, while conducting the solvent-casting with 0.01 wt % solutions of 'ABAB, the polymer chains aggregate into globular cyclic-like aggregates, as shown in Figure 6C-F, while linear chains entangle into a thin network layer (Figure 6A,B). These results are consistent with the reduced chain entanglements of the cyclic topology and

confirm 'ABAB and 'ABAB cyclic and linear topologies, respectively.

Differentiating Di-BCPs and Tetra-BCPs of Similar Block Composition. We first investigated the mechanical performance with differing block complexity. A di-BCP can coentangle across a single copolymer interface (k = 1), while a tetra-BCP can coentangle across multiple points of domain interfaces (k = 3+), acting as multinodal anchors for material self-reinforcement (Figure 7A). In addition, tetra-BCPs are expected to form smaller microdomains due to reduced block volume. These factors should be attributed to increased interfacial adhesion in tetra-BCP samples and enhanced tensile performance. In agreement, the 'AB di-BCP performed poorly with weak ($\sigma_{\rm B}\sim 6$ MPa) and brittle ($\varepsilon_{\rm B}\sim 6\%$) tensile properties and was significantly outperformed by the 'ABAB tetra-BCP, which now registered a yield point, more than doubled tensile strength ($\sigma_{\rm B} \sim 15$ MPa), and a >18-fold increase in ductility ($\varepsilon_{\rm B} \sim 112\%$) (Figures 7B, S43, and S44; Table S3). The ¹AB di-BCP was similarly outperformed by the ABAB tetra-BCP in tensile strength (>2×) and elongation (>20×) (Figures 7C, S45, and S46; Table S3). The 'BCP results, however, are most compelling in that TPE-like behavior is achieved to the extent of lABAB by a ABAB architecture.

Next, we examined self-assembly and microdoman formation and sizing of di- and tetra-BCPs in linear and cyclic topologies. By increasing block count from two to four, while keeping the composition (1/1 mol equiv) and degree of polymerization (DP = 1000) constant, we envisioned that expected self-assembly events would produce ABAB microdomains with \sim 1/2 the size of the AB BCPs. To enhance the effects of self-assembly, as well as to demonstrate the postfunctionalization available through the allylic pendant chain, the thiol—ene click chemistry was used to graft 1-octadecanethiol (1-ODT; $C_{18}H_{37}SH$) crystallizable side chains

onto the PAlA units (Figure 8A). 49,50 Prior to imaging and scattering, we conducted ¹H NMR spectroscopy to verify a disappearance of alkene signals, revealing successful 1-ODT installment (Figures S47 and S48). By DSC, in all four cases, there was no evidence of a PAIA T_g (-35 °C), as well as no shouldering melt temperature (T_m) at ~30 °C which would signal contamination from excess 1-ODT (Figures S49–S53). Lastly, we observed a uniform, one-step decomposition profile in all four 1-ODT-grafted BCPs (Figure 8B).

DSC was revisited to record the $T_{\rm m}$, crystallization temperature (T_c) , enthalpy of crystallization (ΔH_c) , and enthalpy of fusion (ΔH_f) for comparison between the AB di-BCP and ABAB tetra-BCP architectures (Figure 8C,D). In both heating and cooling scans, ${}^{l}BCPs$ had higher T_{m} and T_{c} events than the 'BCPs. For instance, the 'AB di-BCP $T_{\rm m}$ and $T_{\rm c}$ occurred at 51.3 and 37.5 °C, while the 'AB di-BCP $T_{\rm m}$ and $T_{\rm c}$ occurred at 45.9 and 30.9 °C, respectively. In agreement with this correlation, the ¹ABAB tetra-BCP $T_{\rm m}$ and $T_{\rm c}$ were observed at 47.7 and 38.0 °C, higher than the 'ABAB tetra-BCP $T_{\rm m}$ and T_c observed at 45.2 and 29.8 °C, respectively (Figure 8C–E). Shifting in the T_c exotherms (blue) and T_m endotherms (red) highlights the control over BCP crystalline behavior with topology.

We surmised that there may be discrepancies spurred by an architectural sequence such that the di-BCPs would exhibit larger $\Delta H_{\rm f}$ and $\Delta H_{\rm c}$ than the tetra-BCPs due to the larger fraction of the crystalline domain (Figure 8A). This was evident in our experimental results, as integration of both melt and crystallization peaks revealed consistent increases in both $\Delta H_{\rm f}$ and $\Delta H_{\rm c}$ in the di-BCPs compared to the tetra-BCPs (Figure 8E). In the context of topological differences, the $\Delta H_{\rm f}$ and ΔH_c values of the ^lBCPs were ~2× those of the ^cBCPs. Thus, crystallinity is most dependent on the chain packing capacity and is more likely to be disrupted by the cyclic motif.

To evaluate sample morphology, films of the four BCPs were analyzed by TEM (Figure 9), according to the following procedure: thin strips of the samples were put into a RuO₄ solution for 10 min for the staining, followed by ultra cryomicrotoming. RuO₄ stains the polyacrylate (PAIA) segments preferentially, which appear darker on the TEM images (Figure 9). 51,52 On the other hand, PMMA is known to be less affected by RuO_4 , leading to almost unstained domains, depending on staining times. S3-55 Because the length of the crystallizable aliphatic side-chains is around 3 nm, we hypothesize that they are present within the darker (stained) domains of polyacrylate, although a lack of resolution hinders their visualization.

Particularly, a highly ordered phase-segregated morphology is observed for the 'AB di-BCP (Figure 9A), resembling a cylindrical morphology in which the cylindrical dispersed phase is derived from the unstained PMMA amorphous segments. 53-55 This hypothesis arises from the presence of: (1) lower contrast domains that are similar to lamellae, derived from the cross sections parallel to the cylinder's main axis and (2) circular-shaped lower contrast domains, derived from cross sections perpendicular to the cylinders main axis, considering that the TEM provides a 2D-image of a microtomed crosssection of the films.⁵⁶ However, upon a closer view, it is noted that the circular-shaped lower-contrast domains actually possess an elliptical shape (Figure S54), instead of a perfect circular shape expected for a typical cylindrical morphology.⁵ This may arise from morphological differences provided by a cyclic and comb-like morphology.³¹ Regarding the TEM of the

other BCP samples (Figures 9B-D, S55-S57), the morphology resembles disordered lamellae in all cases, with differences in the domain size between the samples, which cannot be precisely determined owing to the disordered nature of the phase-segregated domains.

To allow a better description of the topological and architecture effect over the phase-segregated domain spacing, correlation distances were obtained from SAXS at 25 °C, a temperature at which the TEM measurements were carried out.⁵⁷ Both TEM and X-ray scattering experiments were performed with films that underwent the same thermal treatment. As can be seen in the SAXS plots (Figure \$58), the results obtained for the samples that present a disorganized phase-segregated morphology on TEM (all with the exception of the 'AB) have a low-intensity broad-peak profile, which is even more pronounced for the ABAB tetra-BCPs. The lower intensity of the ABAB tetra-BCPs when compared to the ^lAB di-BCP, all of which have deorganized lamellar phasesegregated morphology, is related to the smaller domain size of the ABAB tetra-BCPs, when compared to the AB di-BCPs, as expected, which is supported by the correlation distance values (Table 1).28,31,55,5

Table 1. Scattering Vector of Maximum Scattering Intensity (q) and Correlation Distances (d) Obtained by SAXS

cAB 0.073 86 lAB 0.06 104 cABAB 0.12 52 lABAB 0.1 63	sample	$q (nm^{-1})$	d (nm)
^c ABAB 0.12 52	^c AB	0.073	86
	^l AB	0.06	104
¹ ABAB 0.1 63	^c ABAB	0.12	52
	^l ABAB	0.1	63

Despite the 'AB organized morphology, the SAXS plot also presents a broad-peak profile, however, narrower than its ^lAB and both ABAB BCP analogues. The broadness of the SAXS scattering peak in the case of 'AB is related to the presence of multiple correlation distances related to distinct chain-packing arrangements throughout the sample, all of which appear in the low-q SAXS range. As visualized by TEM (Figure 9A), the phase-segregated morphology contains cylinders of distinct sizes and shapes (i.e., linear or V-shaped), which are certainly related to the complex cyclic/comb-like architecture of the BCP. 28,57 Therefore, for a more quantitative analysis of the phase-segregated morphology at low-q ranges, a more refined mathematical treatment on the SAXS profile is required and is currently ongoing.⁵⁵ Nevertheless, the organized cylinder-like phase-segregated morphology of the 'AB visualized by TEM (Figure 9A) allows a proper correlation with the data obtained by SAXS, thus providing a basis for hypothesizing a macromolecular arrangement (Figure 10).31,55,57

A scheme of two possible chain conformations of the 'AB, namely, a perfect circle and a fully flat cycle, which possess radii around 40 and 62.5 nm, respectively, is presented in Figure 10. Therefore, the length of a fully flat B-block of aliphatic (1-ODT)-functionalized acrylate is 62.5 nm based on the consideration of a 0.25 nm length per monomeric unit of the acrylate. In Figure 10B, we observed that the length of the dark domains, associated with the semicrystalline acrylicaliphatic comb-like block, is around 60 nm, matching perfectly with a nearly fully flat macromolecular arrangement of the Bblock (acrylic-aliphatic). Because the crystalline lamella is composed of 3 nm length aliphatic chains, they are too small

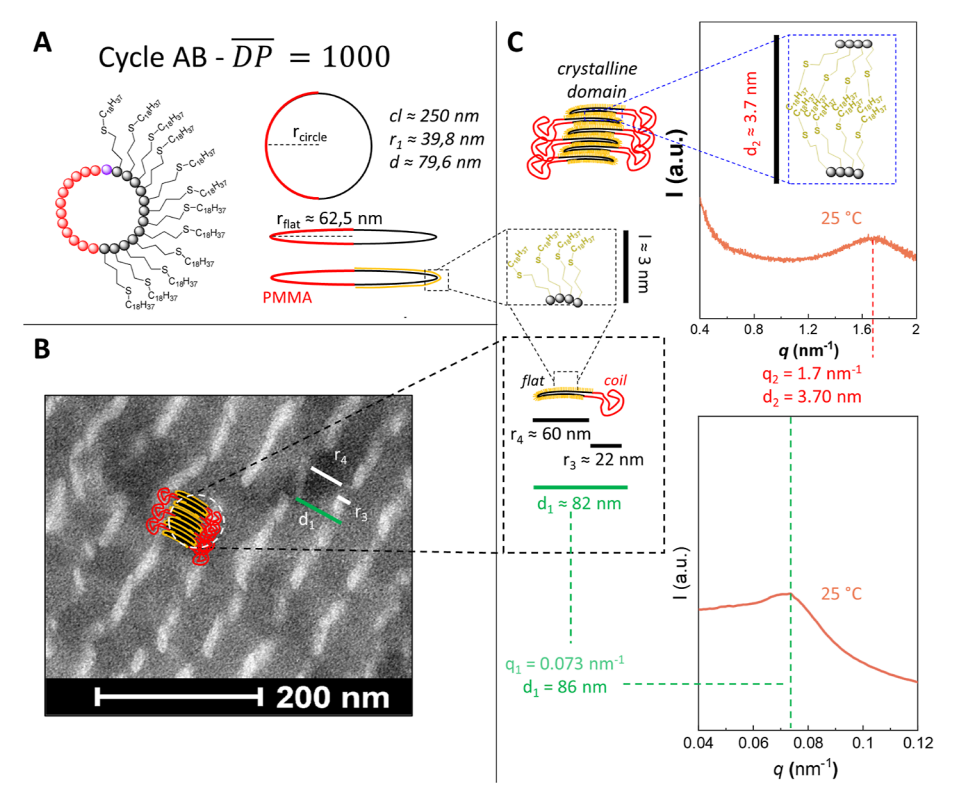


Figure 10. (A) Possible macromolecular arrangements of the 'AB di-BCP with estimated contour-length (cl), and radius of a perfect circular and a flat morphology. (B) TEM image with domain lengths and the scheme of the hypothesized di-BCP chain-packing arrangement. (C) SAXS plots of the 'AB di-BCP with the determined correlation distances and a schematic representation of their correlation with the BCP chain-packing and TEM results.

and cannot be adequately detected within the darker domains of the polyacrylate block.

The 22 nm width of the fully amorphous polymethacrylate domain is probably associated with a random-coil morphology, with lower volume due to its lower molar-volume compared to the aliphatic-functionalized B block. Therefore, the correlation distance obtained by SAXS is presumably related to the length of the 'AB block copolymer on the cylindrical phase-separated morphology, consisting of: (1) a fully flat B-block and (2) a random-coil A block (Figure 10C). This hypothesis is strengthened by the similarity of the chain-length of a hypothetic fully flat 'AB block copolymer arrangement (Figure 10A), domain-length values obtained by TEM (Figure 9B), correlation distance obtained by SAXS (Figure 10C), and volumetric fraction of each BCP block.⁴⁸

On the other hand, SAXS results (Figure 10C) with a ranging from 0.4 to 2 show a broad crystalline peak centered at $q = 1.7 \text{ nm}^{-1}$, which provides a correlation distance d = 3.7 nm, presumably related to the length of the crystalline subdomains composed of aliphatic side chains of the polyacrylate B-block (Figure 10C). This peak is observed for all BCPs and is centered at $q = 1.7 \text{ nm}^{-1}$ for all the samples with the exception of the 'ABAB (Figures S59 and S60). Nevertheless, a length of 3 nm of the aliphatic chains and the correlation distance around 3.7-4 nm provide a strong indication that this peak is related to the crystalline subdomains of packed aliphatic side chains (Figure 10C). Moreover, wide-angle X-ray scattering (WAXS) results confirm the presence of crystalline domains in the four BCP samples by the presence of a crystalline peak centered at $q = 15.2 \text{ nm}^{-1}$ present in the four samples (Figure S61). This peak is more intense in the case of ¹BCPs (Table 1),

indicating a higher degree of crystallinity as already verified by the DSC analysis (Figure 8E). This peak corresponds to a 2θ value of 21.4°, which is the same value reported in the literature for the reflection of the plane (110) of the polyethylene in the monoclinic unit cell form ^{59,60} of the poly(oxidodecamethylene). Therefore, the crystalline component of the BCPs is due to the crystallization of the aliphatic (1-ODT) side chains of the polyacrylate block, and the cyclic topology of the 'AB and 'ABAB architectures partially hinders such crystallization.

CONCLUSIONS

In summary, we report on the synthesis and characterization of complex linear and cyclic tetra-BCPs from mixed-feed (meth)acrylate monomers in a one-pot, two-step polymerization procedure in a speedy, scalable manner. The precision of this method is also specifically highlighted by the accessibility of a 'ABAB tetra-BCP with block symmetry of 25/25.5/25/24.5 and $M_n = 168$ kg mol⁻¹ (D = 1.18), along with its linear counterpart ¹ABAB tetra-BCP with a block symmetry of 25/27.5/25/22.5 and $M_n = 165 \text{ kg mol}^{-1}$ (D = 1.25), both of which were prepared at about 40 g and <15 min. Distinctions between the linear and cyclic tetra-BCPs are recorded, while corroborated with behavioral patterns between well-documented linear and cyclic AB di-BCPs. Multilevel characterizations in different BCP states designed to differentiate between the two MBCP topologies collected several lines of evidence that corraboratively confirmed their topological assignments. Consistent with these assignments, key distinctions are revealed to show that, as compared to its linear tetra-BCP counterpart, the 'ABAB tetra-BCP exhibits

clearly differentiated properties in solution (a smaller hydrodynamic volume, lower solution viscosity, longer elution time, and lower refractive index); bulk (a higher onset decomposition temperature and glass-transition temperature); and film (a higher dynamic storage modulus and a considerably higher fracture strain). Further distinctions were revealed by rheological flow experiments that showed a lower melt viscosity for 'ABAB tetra-BCP, while AFM analysis clearly depicted circular ring shapes for the 'ABAB and a webbed layout for the lABAB analogue as direct imaging evidence for the topology assignments.

The precision synthesis of both linear and cyclic MBCPs enabled by CSC-LPP also presented a unique opportunity for studying architectural effects of di- and tetra-BCPs with the same comonomer composition and molecular weight. Key findings include: (1) tetra-BCPs, regardless of topology, exhibit notably higher tensile toughness than di-BCPs, thanks to TPE interdomain entanglements within networks of tetra-BCPs and (2) self-assembly and microdomain phase segregation are promoted via alkene functionalization by the large crystalline pendant groups. Domain spacing is substantially reduced by around 40% with an increase in block number from 2 to 4 in both linear and cyclic BCPs.

We emphasize that CSC-LPP can be exploited to create more diverse and architecturally complex MBCPs within and beyond linear topology, for which exploration and implementation is still ongoing for even more intricate architecturally coupled topological structures. As MBCPs continue to emerge as superior alternatives to di-BCPs in fields requiring smaller domain sizes and stronger interdomain entanglements, the need for scalability in appreciable timeframes will become more crucial to their adoption and application.

ASSOCIATED CONTENT

Supporting Information

The Supporting Information is available free of charge at https://pubs.acs.org/doi/10.1021/jacs.3c14136.

Materials, methods, and reagents; analysis and instrumentation details; polymerization procedures and postsynthetic modification protocols; H NMR, C NMR, batch dn/dc measurement result, GPC, TGA, DSC, DMA curves, rheometric flow curve, AFM, stress–strain curve, TEM, SAXS, WAXS, DMA temperatureramp frequency sweep data, rheometric flow analysis table, and tensile (stress/strain) testing averaged data (PDF)

AUTHOR INFORMATION

Corresponding Authors

Alejandro J. Müller — Polymat and Department of Polymers and Advanced Materials: Physics, Chemistry and Technology, Faculty of Chemistry, University of the Basque Country UPV/EHU, Donostia-San Sebastián 20018, Spain; IKERBASQUE, Basque Foundation for Science, Bilbao 48009, Spain; orcid.org/0000-0001-7009-7715; Email: alejandrojesus.muller@ehu.es

Eugene Y.-X. Chen — Department of Chemistry, Colorado State University, Fort Collins, Colorado 80523-1872, United States; orcid.org/0000-0001-7512-3484; Email: eugene.chen@colostate.edu

Authors

Ryan W. Clarke – Department of Chemistry, Colorado State University, Fort Collins, Colorado 80523-1872, United States

Maria Rosaria Caputo – Polymat and Department of Polymers and Advanced Materials: Physics, Chemistry and Technology, Faculty of Chemistry, University of the Basque Country UPV/EHU, Donostia-San Sebastián 20018, Spain

Lucas Polo Fonseca — Polymat and Department of Polymers and Advanced Materials: Physics, Chemistry and Technology, Faculty of Chemistry, University of the Basque Country UPV/EHU, Donostia-San Sebastián 20018, Spain

Michael L. McGraw – Department of Chemistry, Colorado State University, Fort Collins, Colorado 80523-1872, United States

Liam T. Reilly – Department of Chemistry, Colorado State University, Fort Collins, Colorado 80523-1872, United States; o orcid.org/0000-0003-1469-7606

Kevin A. Franklin — Department of Chemistry, Colorado State University, Fort Collins, Colorado 80523-1872, United States

Complete contact information is available at: https://pubs.acs.org/10.1021/jacs.3c14136

Notes

The authors declare no competing financial interest.

ACKNOWLEDGMENTS

The work done at CSU was supported in part by the U.S. National Science Foundation (NSF-2305058) and by the US Army Research Office (W911NF2310123). The researchers at UPV/EHU thank the ALBA synchrotron for funding (granted proposal no. 2022025606), facilities, and staff support, acknowledge project PID2020-113045GB-C21 funded by MCINN/AEI/10.13039/501100011033 and grant IT1503-22 by the Basque Government, and thank the technical and human support provided by SGIker (UPV/EHU/ERDF, EU). L.P.F. thanks the ADAGIO: Advanced Manufacturing Research Fellowship Program in the Basque New Aquitaine Region.

REFERENCES

- (1) Liénard, R.; De Winter, J.; Coulembier, O. Cyclic Polymers: Advances in Their Synthesis, Properties, and Biomedical Applications. *J. Polym. Sci.* **2020**, *58*, 1481–1502.
- (2) Haque, F. M.; Grayson, S. M. The Synthesis, Properties and Potential Applications of Cyclic Polymers. *Nat. Chem.* **2020**, *12*, 433–444
- (3) Kricheldorf, H. R. Cyclic Polymers: Synthetic Strategies and Physical Properties. J. Polym. Sci., Part A: Polym. Chem. 2010, 48, 251–284.
- (4) Zhu, Y.; Hosmane, N. S. Advanced Developments in Cyclic Polymers: Synthesis, Applications, and Perspectives. *ChemistryOpen* **2015**, *4*, 408–417.
- (5) Yamamoto, T.; Tezuka, Y. Topological Polymer Chemistry: A Cyclic Approach toward Novel Polymer Properties and Functions. *Polym. Chem.* **2011**, *2*, 1930–1941.
- (6) Romio, M.; Trachsel, L.; Morgese, G.; Ramakrishna, S. N.; Spencer, N. D.; Benetti, E. M. Topological Polymer Chemistry Enters Materials Science: Expanding the Applicability of Cyclic Polymers. *ACS Macro Lett.* **2020**, *9*, 1024–1033.
- (7) Bielawski, C. W.; Benitez, D.; Grubbs, R. H. An "Endless" Route to Cyclic Polymers. *Science* **2002**, *297*, 2041–2044.
- (8) Wang, T.-W.; Golder, M. R. Advancing macromolecular hoop construction: recent developments in synthetic cyclic polymer chemistry. *Polym. Chem.* **2021**, *12*, 958–969.

- (9) Tezuka, Y. Topological Polymer Chemistry: Progress of Cyclic Polymers in Syntheses, Properties, and Functions; Word Scientific Publishing Company, 2013.
- (10) Roovers, J. Organic Cyclic Polymers. In *Cyclic Polymers*; Semlyen, J. A., Ed.; Kluwer Academic Press: Dordrecht, Boston, London, 2000; Chapter 10, pp 347–385.
- (11) Hadziioannou, G.; Cotts, P. M.; ten Brinke, G.; Han, C. C.; Lutz, P.; Strazielle, C.; Rempp, P.; Kovacs, A. J. Thermodynamic and Hydrodynamic Properties of Dilute Solutions of Cyclic and Linear Polystyrenes. *Macromolecules* **1987**, *20*, 493–497.
- (12) Song, Y.; He, J.; Zhang, Y.; Gilsdorf, R. A.; Chen, E. Y.-X. Recyclable Cyclic Bio-based Acrylic Polymer via Pairwise Monomer Enchainment by a Trifunctional Lewis Pair. *Nat. Chem.* **2023**, *15*, 366–376.
- (13) Honda, S.; Yamamoto, T.; Tezuka, Y. Topology-Directed Control on Thermal Stability: Micelles Formed from Linear and Cyclized Amphiphilic Block Copolymers. *J. Am. Chem. Soc.* **2010**, *132*, 10251–10253.
- (14) Li, H.; Ollivier, J.; Guillaume, S. M.; Carpentier, J. F. Tacticity Control of Cyclic Poly(3-Thiobutyrate) Prepared by Ring-Opening Polymerization of Racemic β -Thiobutyrolactone. *Angew. Chem., Int. Ed.* **2022**, *61*, No. e2022023.
- (15) Santangelo, P. G.; Roland, C. M. Molecular Weight Dependence of Fragility in Polystyrene. *Macromolecules* **1998**, *31*, 4581–4585.
- (16) Hong, M.; Chen, E. Y. X. Completely Recyclable Biopolymers with Linear and Cyclic Topologies via Ring-Opening Polymerization of γ-Butyrolactone. *Nat. Chem.* **2016**, *8*, 42–49.
- (17) Córdova, M. E.; Lorenzo, A. T.; Müller, A. J.; Hoskins, J. N.; Grayson, S. M. A Comparative Study on the Crystallization Behavior of Analogous Linear and Cyclic Poly(ε -Caprolactones). *Macromolecules* **2011**, *44*, 1742–1746.
- (18) Shin, E. J.; Jeong, W.; Brown, H. A.; Koo, B. J.; Hedrick, J. L.; Waymouth, R. M. Crystallization of Cyclic Polymers: Synthesis and Crystallization Behavior of High Molecular Weight Cyclic Poly(ε -Caprolactone)S. *Macromolecules* **2011**, *44*, 2773–2779.
- (19) Pérez-Camargo, R. A.; Mugica, A.; Zubitur, M.; Müller, A. J. Crystallization of Cyclic Polymers. *Adv. Polym. Sci.* **2015**, 276, 93–132.
- (20) Roovers, J. Viscoelastic Properties of Polybutadiene Rings. *Macromolecules* **1988**, *21*, 1517–1521.
- (21) Kapnistos, M.; Lang, M.; Vlassopoulos, D.; Pyckhout-Hintzen, W.; Richter, D.; Cho, D.; Chang, T.; Rubinstein, M. Unexpected Power-Law Stress Relaxation of Entangled Ring Polymers. *Nat. Mater.* **2008**, *7*, 997–1002.
- (22) Pasquino, R.; Vasilakopoulos, T. C.; Jeong, Y. C.; Lee, H.; Rogers, S.; Sakellariou, G.; Allgaier, J.; Takano, A.; Brás, A. R.; Chang, T.; Gooßen, S.; Pyckhout-Hintzen, W.; Wischnewski, A.; Hadjichristidis, N.; Richter, D.; Rubinstein, M.; Vlassopoulos, D. Viscosity of Ring Polymer Melts. ACS Macro Lett. 2013, 2, 874–878.
- (23) He, T.; Zheng, G. H.; Pan, C. Y. Synthesis of Cyclic Polymers and Block Copolymers by Monomer Insertion into Cyclic Initiator by a Radical Mechanism. *Macromolecules* **2003**, *36*, 5960–5966.
- (24) Piedra-Arroni, E.; Ladavière, C.; Amgoune, A.; Bourissou, D. Ring-Opening Polymerization with $Zn(C_6F_5)_2$ -Based Lewis Pairs: Original and Efficient Approach to Cyclic Polyesters. *J. Am. Chem. Soc.* **2013**, *135*, 13306–13309.
- (25) Yin, R.; Hogen-Esch, T. E. Synthesis and Characterization of Narrow Molecular Weight Distribution Polystyrene-Poly-(Dimethylsiloxane) Macrocyclic Block Copolymers and Their Isobaric Precursors. *Macromolecules* 1993, 26, 6952–6957.
- (26) Wagener, K. B.; Smith, D. W. Acyclic Diene Metathesis Polymerization. Synthesis and Characterization of Unsaturated Poly[Carbo(Dimethyl)Silanes]. *Macromolecules* **1991**, *24*, 6073–6078
- (27) Deffieux, A.; Schappacher, M.; Rique-Lurbet, L. New Routes to Macrocyclic Polymers of Controlled Dimensions. *Polymer* **1994**, *35*, 4562–4568.

- (28) Lecommandoux, S.; Borsali, R.; Schappacher, M.; Deffieux, A.; Narayanan, T.; Rochas, C. Microphase Separation of Linear and Cyclic Block Copolymers Poly(Styrene-b-Isoprene): SAXS Experiments. *Macromolecules* **2004**, *37*, 1843–1848.
- (29) Koo, M. B.; Lee, S. W.; Lee, J. M.; Kim, K. T. Iterative Convergent Synthesis of Large Cyclic Polymers and Block Copolymers with Discrete Molecular Weights. *J. Am. Chem. Soc.* **2020**, *142*, 14028–14032.
- (30) Zhang, B.; Zhang, H.; Li, Y.; Hoskins, J. N.; Grayson, S. M. Exploring the Effect of Amphiphilic Polymer Architecture: Synthesis, Characterization, and Self-Assembly of Both Cyclic and Linear Poly(Ethylene Gylcol)- B -Polycaprolactone. *ACS Macro Lett.* **2013**, 2, 845–848.
- (31) Williams, R. J.; Dove, A. P.; O'Reilly, R. K. Self-Assembly of Cyclic Polymers. *Polym. Chem.* **2015**, *6*, 2998–3008.
- (32) Polymeropoulos, G.; Zapsas, G.; Ntetsikas, K.; Bilalis, P.; Gnanou, Y.; Hadjichristidis, N. 50th Anniversary Perspective: Polymers with Complex Architectures. *Macromolecules* **2017**, *50*, 1253–1290.
- (33) Polymeropoulos, G.; Bilalis, P.; Hadjichristidis, N. Well-Defined Cyclic Triblock Terpolymers: A Missing Piece of the Morphology Puzzle. ACS Macro Lett. 2016, 5, 1242–1246.
- (34) Chuang, V. P.; Ross, C. a.; Bilalis, P.; Hadjichristidis, N. Nanoscale Rings Fabricated Using Self-Assembled Triblock Terpolymer Templates. *ACS Nano* **2008**, *2*, 2007–2014.
- (35) Luo, M.; Epps, T. H. Directed Block Copolymer Thin Film Self-Assembly: Emerging Trends in Nanopattern Fabrication. *Macromolecules* **2013**, *46*, 7567–7579.
- (36) Poelma, J. E.; Ono, K.; Miyajima, D.; Aida, T.; Satoh, K.; Hawker, C. J. Cyclic Block Copolymers for Controlling Feature Sizes in Block Copolymer Lithography. *ACS Nano* **2012**, *6*, 10845–10854.
- (37) Tu, X. Y.; Liu, M. Z.; Wei, H. Recent Progress on Cyclic Polymers: Synthesis, Bioproperties, and Biomedical Applications. *J. Polym. Sci., Part A: Polym. Chem.* **2016**, *54*, 1447–1458.
- (38) Creton, C.; Kramer, E. J.; Hui, C. Y.; Brown, H. R. Failure Mechanisms of Polymer Interfaces Reinforced with Block Copolymers. *Macromolecules* **1992**, *25*, 3075–3088.
- (39) Self, J. L.; Zervoudakis, A. J.; Peng, X.; Lenart, W. R.; Macosko, C. W.; Ellison, C. J. Linear, Graft, and Beyond: Multiblock Copolymers as Next-Generation Compatibilizers. *JACS Au* **2022**, *2*, 310–321.
- (40) Xu, J.; Eagan, J. M.; Kim, S. S.; Pan, S.; Lee, B.; Klimovica, K.; Jin, K.; Lin, T. W.; Howard, M. J.; Ellison, C. J.; Lapointe, A. M.; Coates, G. W.; Bates, F. S. Compatibilization of Isotactic Polypropylene (IPP) and High-Density Polyethylene (HDPE) with IPP-PE Multiblock Copolymers. *Macromolecules* **2018**, *51*, 8585–8596
- (41) Eagan, J. M.; Xu, J.; Di Girolamo, R.; Thurber, C. M.; Macosko, C. W.; La Pointe, A. M.; Bates, F. S.; Coates, G. W. Combining Polyethylene and Polypropylene: Enhanced Performance with PE/IPP Multiblock Polymers. *Science* **2017**, *355*, 814–816.
- (42) Laurent, B. A.; Grayson, S. M. Synthetic Approaches for the Preparation of Cyclic Polymers. *Chem. Soc. Rev.* **2009**, *38*, 2202–2213.
- (43) McGraw, M. L.; Clarke, R. W.; Chen, E. Y. X. Compounded Sequence Control in Polymerization of One-Pot Mixtures of Highly Reactive Acrylates by Differentiating Lewis Pairs. *J. Am. Chem. Soc.* **2020**, *142*, 5969–5973.
- (44) McGraw, M. L.; Clarke, R. W.; Chen, E. Y. X. Synchronous Control of Chain Length/Sequence/Topology for Precision Synthesis of Cyclic Block Copolymers from Monomer Mixtures. *J. Am. Chem. Soc.* **2021**, *143*, 3318–3322.
- (45) McGraw, M. L.; Chen, E. Y.-X. Lewis Pair Polymerization: Perspective on a Ten-Year Journey. *Macromolecules* **2020**, *53*, 6102–6122.
- (46) McGraw, M. L.; Reilly, L. T.; Clarke, R. W.; Cavallo, L.; Falivene, L.; Chen, E. Y. X. Mechanism of Spatial and Temporal Control in Precision Cyclic Vinyl Polymer Synthesis by Lewis Pair Polymerization. *Angew. Chem., Int. Ed.* **2022**, *61*, No. e202116303.

- (47) Reilly, L. T.; McGraw, M. L.; Eckstrom, F. D.; Clarke, R. W.; Franklin, K. A.; Chokkapu, E. R.; Cavallo, L.; Falivene, L.; Chen, E. Y.-X. Compounded Interplay of Kinetic and Thermodynamic Control over Comonomer Sequences by Lewis Pair Polymerization. *J. Am. Chem. Soc.* **2022**, *144*, 23572–23584.
- (48) Saito, Y.; Lien, L. T. N.; Jinbo, Y.; Kumaki, J.; Narumi, A.; Kawaguchi, S. Influence of the Primary Structure of the Main Chain on Backbone Stiffness of Cylindrical Rod Brushes. *Polym. J.* **2013**, *45*, 193–201.
- (49) Naruse, K.; Takasu, A.; Higuchi, M. Direct Observation of a Cyclic Vinyl Polymer Prepared by Anionic Polymerization Using N-Heterocyclic Carbene and Subsequent Ring-Closure without Highly Diluted Conditions. *Macromol. Chem. Phys.* **2020**, *221*, 2000004.
- (50) Muramatsu, Y.; Takasu, A.; Higuchi, M.; Hayashi, M. Direct observation of the formation of a cyclic poly(alkyl sorbate) via chaingrowth polymerization by an *N*-heterocyclic carbene initiator and ring-closing without extreme dilution. *J. Polym. Sci.* **2020**, 58, 2936—2942
- (51) Trent, J. S. Ruthenium Tetraoxide Staining of Polymers: New Preparative Methods for Electron Microscopy. *Macromolecules* **1984**, *17*, 2930–2931.
- (52) Stadler, R.; Auschra, C.; Beckmann, J.; Krappe, U.; Voight-Martin, I.; Leibler, L. Morphology and Thermodynamics of Symmetric Poly(A-Block-B-Block-C) Triblock Copolymers. *Macromolecules* 1995, 28, 3080–3097.
- (53) Brinkmann, S.; Stadler, R.; Thomas, E. L. New Structural Motif in Hexagonally Ordered Cylindrical Ternary (ABC) Block Copolymer Microdomains. *Macromolecules* **1998**, *31*, 6566–6572.
- (54) Kang, J.; Beers, K. J. Effect of Temperature and Water on Microphase Separation of PCL-PEO-PCL Triblock Copolymers. *Polym. Bull.* **2009**, *63*, 723–734.
- (55) Mai, Y.; Eisenberg, A. Self-Assembly of Block Copolymers. Chem. Soc. Rev. 2012, 41, 5969-5985.
- (56) Eaton, P.; Quaresma, P.; Soares, C.; Neves, C.; de Almeida, M. P.; Pereira, E.; West, P. A Direct Comparison of Experimental Methods to Measure Dimensions of Synthetic Nanoparticles. *Ultramicroscopy* **2017**, *182*, 179–190.
- (57) Borsali, R.; Pecora, R. Soft Matter Characterization; Springer, 2008.
- (58) da Silva, L. C. E.; Plivelic, T. S.; do Carmo Gonçalves, M. Morphological Investigation of Ternary and Semicrystalline Organic—Inorganic Hybrid Nanocomposite. *J. Mater. Sci.* **2022**, *57*, 6196–6211.
- (59) Mark, J. E. Physical Properties of Polymers Handbook, 2nd ed.; Springer: New York, 2006.
- (60) Russell, K. E.; Hunter, B. K.; Heyding, R. D. Monoclinic Polyethylene Revisited. *Polymer* **1997**, *38*, 1409–1414.
- (61) Basterretxea, A.; Gabirondo, E.; Flores, I.; Etxeberria, A.; Gonzalez, A.; Müller, A. J.; Mecerreyes, D.; Coulembier, O.; Sardon, H. Isomorphic Polyoxyalkylene Copolyethers Obtained by Copolymerization of Aliphatic Diols. *Macromolecules* **2019**, *52*, 3506–3515.